Engineering Transactions, **71**(1): 81–109, 2023, doi: 10.24423/EngTrans.2456.20230126
Institute of Fundamental Technological Research Polish Academy of Sciences (IPPT PAN)
Université de Lorraine • Poznan University of Technology

Research Paper

A Parametric Study of Higher-Mode Natural Frequencies of Composite Stiffened Cylindrical Shell With Cut-Out

Puja BASU CHAUDHURI[1)], Anirban MITRA[2)], Sarmila SAHOO[1)*]

[1)] *Department of Civil Engineering, Heritage Institute of Technology*
Kolkata 700107, India

[2)] *Department of Mechanical Engineering, Jadavpur University*
Kolkata 700032, India

[*]Corresponding Author e-mail: sarmila.sahoo@gmail.com; sarmila.sahoo@heritageit.edu

A finite element-based dynamic study of cut-out borne composite cylindrical shells reinforced with stiffeners is conducted. Isoparametric shell element with eight nodes and beam element with three nodes are used to study the mode-frequency behavior of shells with varied edge conditions. Anti-symmetric angle-ply laminates of two, four and ten layers with varying lamination angles are considered. Ten-layer laminates are investigated further as they exhibit better performance in fundamental frequency than two and four-layer laminates. The reduced integration method is adopted to find the shell element's stiffness and mass matrices and the subspace iteration method is used for the eigenvalue solution of free vibration formulation. Natural frequencies for the first five modes are considered. The effects of fiber orientation angle (θ), degree of orthotropy (E_{11}/E_{22}), and width/thickness ratio (b/h) on the natural frequency are determined through numerical studies. It is revealed that vibration behavior strongly depends on both the number and arrangement of boundary constraints.

Keywords: stiffener; cylindrical shell; cut-out; laminated composite; finite element; natural frequency.

1. Introduction

The cylindrical shell structures find wide use as a fundamental structural member in different engineering applications in civil, mechanical and aerospace engineering. Earlier such shell forms were made of conventional materials such as steel. However, the dead weight of steel shells is high; thus, laminated composites replace steel shells to take advantage of their large specific strength and stiffness values. Accordingly, laminated composites have gained popularity in weight-sensitive engineering uses. In civil and architectural constructions, large column-free open area is covered by cylindrical roofing structures since they are

easily fabricated. Laminated composite shell structures often include cut-outs for the placement of windows, doors, inspection accessories, etc. Cut-outs are incorporated deliberately sometimes as a means for avoiding resonance criteria. The presence of cut-out imperfections leads to substantial stress concentrations and, in turn, influences the dynamic and stability characteristics. Accordingly, such cylindrical shells are typically stiffened along the boundaries of the cut-out imperfections.

Laminated composite structures can improve different attributes of the structure by suitable modification of the sequential stacking of the layers. Such provision is generally absent in other kinds of structures. Moreover, laminated structures can combine the best attributes of the component layers to tailor appropriate improved characteristics of the complete structure by way of judicious choice of materials for different layers. Accordingly, the study of laminated structures has gained importance in practical applications. The stability characteristics of structures having cut-outs pose a hindrance to structural designers who need to have prior knowledge of the dynamic response of structures. This aspect of laminated composite structures in the presence of cut-outs has attracted the attention of researchers who have utilized various methodologies for such analysis. Considering the cost of any experimental study for such structures with imperfections, the finite element (FE) analysis has emerged as a viable alternative for determining structural responses in terms of vibration and stability. Ritz's minimization technique was extensively used for the evaluation of the natural frequency and mode shapes for different shell geometries [1–4] and even for pre-twisted cantilever trapezoidal laminates [5]. Recent studies on vibration aspects have been reviewed as well [6]. Vibration studies of cut-out borne curved panels [7] and stiffened square panels [8] were also reported. Higher-order shear deformation theory was used for the free vibration study of cut-out borne spherical shells [9] to evaluate the impact of plies, radius/thickness ratio, edge constraints and cut-out size. Free vibration of cut-out borne conoidal stiffened shell was also analyzed [10]. Plate with different shapes of cut-outs was analyzed for vibration behavior [11].

Composite cylindrical shell panel under nonlinear vibration was also reported [12] to consider the effect of aspect ratios, lamination, cut-out and material for simply supported edge condition. Laminated hyperbolic-paraboloid (hypar) shell was studied for free vibration behavior [13] in the presence of cut-out using the FE procedure. Higher order shear deformation theory and Sander's approximation were utilized to consider a nine-noded curved C_0 FE formulation for the dynamic study of composite shells with cut-outs [14]. The sampling surface technique was extended to consider the 3D elasticity solutions in cylindrical and spherical composite shells [15]. Talebitooti *et al.* [16] considered the acoustic response of composite cylindrical shells under excitation

by an oblique sound wave. The vibration of doubly curved shells with variable thickness has also been analyzed [17, 18]. Doubly curved shell panels with elastic restraints have been considered for free vibration [19]. Innovative higher-order theory [20] has been used to accurately evaluate natural frequencies.

Thus it is revealed from the review of available literature that free vibration of stiffened cylindrical shells with cut-outs has been reported in different studies to evaluate various parametric combinations. However, no study is available on the higher-mode vibration behavior of cylindrical shells with cut-outs. A recent study [21] of anti-symmetric angle-ply laminated composite hypar shells (hyperbolic paraboloid bounded by straight edges) presented mode-frequency analysis of stiffened shell with cut-out. It remains unexplored whether the higher mode vibration behavior of shells is specific to shell geometry or if some generalized behavioral pattern exists for different shell geometries. Thus, the aim of the current study is two-fold. First, it attempts to provide information on the higher-mode free vibration aspect of cylindrical shells with a cut-out, which is missing in the literature. Secondly, it aims to compare the same with available results [21] for another type of shell, namely, a hypar shell with cut-out. Accordingly, the dependence of higher-mode natural frequencies on width/thickness ratio (b/h), degree of orthotropy (E_{11}/E_{22}), and fiber orientation angle (θ) for cut-out borne stiffened cylindrical shell with 10-layer laminates is evaluated for different edge conditions used in practical applications.

2. Mathematical formulation

A laminated shell is composed of a large number of orthotropic layers, each having uniform thickness, and orientation may be arbitrary with the shell coordinates (ξ_1, ξ_2, ς). Here the shell is considered to have an orthogonal curvilinear coordinate system (ξ_1, ξ_2, ς), where the ξ_1 and ξ_2-curves are lines of curvature on the mid-surface, $\varsigma = 0$, and ς-axes are straight lines perpendicular to the surface $\varsigma = 0$ (Fig. 1). Considering the shear deformation, the strain-displacement relations for doubly curved shells are given by [22]

$$
\begin{aligned}
\varepsilon_1 &= \varepsilon_1^0 + \varsigma\kappa_1, \\
\varepsilon_2 &= \varepsilon_2^0 + \varsigma\kappa_2, \\
\varepsilon_4 &= \varepsilon_4^0, \\
\varepsilon_5 &= \varepsilon_5^0, \\
\varepsilon_6 &= \varepsilon_6^0 + \varsigma\kappa_6,
\end{aligned}
\tag{2.1}
$$

where

$$\varepsilon_1^0 = \frac{\partial u}{\partial x} + \frac{w}{R_x}, \qquad \kappa_1 = \frac{\partial \alpha}{\partial x},$$
$$\varepsilon_2^0 = \frac{\partial v}{\partial y} + \frac{w}{R_y}, \qquad \kappa_2 = \frac{\partial \beta}{\partial y},$$
$$\varepsilon_6^0 = \frac{\partial u}{\partial y} + \frac{\partial v}{\partial x} + \frac{2w}{R_{xy}}, \qquad \kappa_6 = \frac{\partial \alpha}{\partial y} + \frac{\partial \beta}{\partial x} - C_0\left(\frac{\partial v}{\partial x} - \frac{\partial u}{\partial y}\right),$$
$$\varepsilon_4^0 = \beta + \frac{\partial w}{\partial y} - \frac{v}{R_y}, \qquad \varepsilon_5^0 = \alpha + \frac{\partial w}{\partial x} - \frac{u}{R_x},$$
$$C_0 = \frac{1}{2}\left(\frac{1}{R_x} - \frac{1}{R_y}\right), \qquad \mathrm{d}x = \theta_1\,\mathrm{d}\xi_1, \qquad \mathrm{d}y = \theta_2\,\mathrm{d}\xi_2.$$

Here, u, v, w represent the displacements in the directions of ξ_1, ξ_2, and ς axes, and α, β denote the rotations of transverse normals about the ξ_1, ξ_2 axes, respectively. The C_0 term results from Sanders' theory to consider the zero strain condition as applicable for rigid body motion.

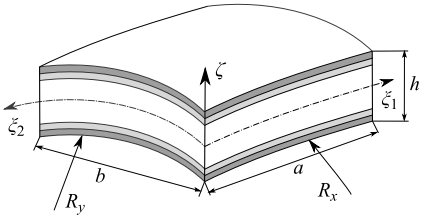

FIG. 1. Geometry of a doubly curved shell.

2.1. Governing equations

Considering the effect of shear deformation for the doubly curved panel, free vibration is governed by the following equations [23, 24]:

$$\begin{aligned}
\frac{\partial N_1}{\partial x} + \frac{\partial}{\partial y}\left(N_6 + C_0 M_6\right) + \frac{Q_1}{R_x} &= P_1\frac{\partial^2 u}{\partial t^2} + P_2\frac{\partial^2 \alpha}{\partial t^2},\\
\frac{\partial}{\partial x}\left(N_6 - C_0 M_6\right) + \frac{\partial N_2}{\partial y} + \frac{Q_2}{R_y} &= \overline{P}_1\frac{\partial^2 v}{\partial t^2} + \overline{P}_2\frac{\partial^2 \beta}{\partial t^2},\\
\frac{\partial \alpha}{\partial x} + \frac{\partial \beta}{\partial y} - \left(\frac{N_1}{R_x} + \frac{N_2}{R_y}\right) &= I_1\frac{\partial^2 w}{\partial t^2},\\
\frac{\partial M_1}{\partial x} + \frac{\partial M_6}{\partial y} - Q_1 &= I_3\frac{\partial^2 \alpha}{\partial t^2} + P_2\frac{\partial^2 u}{\partial t^2},\\
\frac{\partial M_6}{\partial x} + \frac{\partial M_2}{\partial y} - Q_2 &= I_3\frac{\partial^2 \beta}{\partial t^2} + \overline{P}_2\frac{\partial^2 v}{\partial t^2},
\end{aligned} \tag{2.2}$$

where N_i and M_i represent the stress and moment resultants, respectively, whereas Q_i are the shear force resultants:

$$(N_i, M_i) = \sum_{k=1}^{L} \int_{\varsigma_{k-1}}^{\varsigma_k} \sigma_i \, (1, \varsigma) \, \mathrm{d}\varsigma, \qquad i = 1, 2, 6,$$

$$(Q_1, Q_2) = \sum_{k=1}^{L} \int_{\varsigma_{k-1}}^{\varsigma_k} \left(K_1^2 \sigma_5, K_2^2 \sigma_4\right) \mathrm{d}\varsigma.$$

Here K_i^2 $(i = 1, 2)$ denote the correction factors for shear deformation, and the resultants $(N_i,\, M_i,\, Q_i)$ may be related to $(\varepsilon_i,\, \kappa_i)$ by

$$\begin{aligned} N_i &= A_{ij}\varepsilon_i^0 + B_{ij}\kappa_i, \qquad i, j = 1, 2, 6, \\ M_i &= B_{ij}\varepsilon_i^0 + D_{ij}\kappa_i, \\ Q_1 &= A_{45}\varepsilon_4^0 + A_{55}\varepsilon_5^0, \\ Q_2 &= A_{44}\varepsilon_4^0 + A_{45}\varepsilon_5^0, \end{aligned} \tag{2.3}$$

where A_{ij}, B_{ij}, and D_{ij} specify stiffness due to extension, flexure-extension coupling and flexure, respectively, for the laminates. Details of the elasticity matrix are available in [25, 26]

$$(A_{ij}, B_{ij}, D_{ij}) = \sum_{k=1}^{L} \int_{\varsigma_{k-1}}^{\varsigma_k} Q_{ij} \left(1, \varsigma, \varsigma^2\right) \mathrm{d}\varsigma,$$

and the shear coefficients are

$$(A_{44}, A_{45}, A_{55}) = \sum_{k=1}^{L} \int_{\varsigma_{k-1}}^{\varsigma_k} \left(K_1^2 Q_{44}, K_1 K_2 Q_{45}, K_2^2 Q_{55}\right) \mathrm{d}\varsigma,$$

P_i are the inertias:

$$(P_1, P_2, P_3) = \sum_{k=1}^{L} \int_{\varsigma_{k-1}}^{\varsigma_k} \rho^k \left(1, \varsigma, \varsigma^2\right) \mathrm{d}\varsigma,$$

$$P_1 = I_1 + \frac{2I_2}{R_x}, \qquad P_2 = I_2 + \frac{I_3}{R_y},$$

$$\overline{P}_1 = I_1 + \frac{2I_2}{R_y}, \qquad \overline{P}_2 = I_2 + \frac{I_3}{R_x},$$

where

$$(I_1, I_2, I_3) = \sum_{k=1}^{L} \int_{\varsigma_{k-1}}^{\varsigma_k} \varsigma^k \left(1, \rho, \rho^2\right) \mathrm{d}\varsigma,$$

and L denotes the total number of layers present.

2.2. Finite element model

For the present analysis of the cylindrical shell panel (Fig. 2), an eight-noded curved quadratic isoparametric finite element (Fig. 3) is used. The five degrees of freedom taken into consideration at each node are u, v, w, α, β. The following expressions establish the relations between the displacement at any point with respect to the co-ordinates ξ and η and the nodal degrees of freedom.

$$u = \sum_{i=1}^{8} N_i u_i, \quad v = \sum_{i=1}^{8} N_i v_i, \quad w = \sum_{i=1}^{8} N_i w_i, \quad \alpha = \sum_{i=1}^{8} N_i \alpha_i, \quad \beta = \sum_{i=1}^{8} N_i \beta_i, \tag{2.4}$$

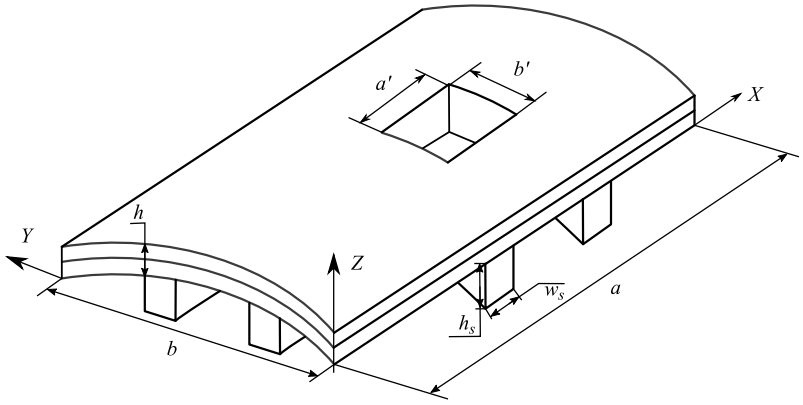

FIG. 2. Cylindrical shell with a concentric cut-out stiffened along the margins.

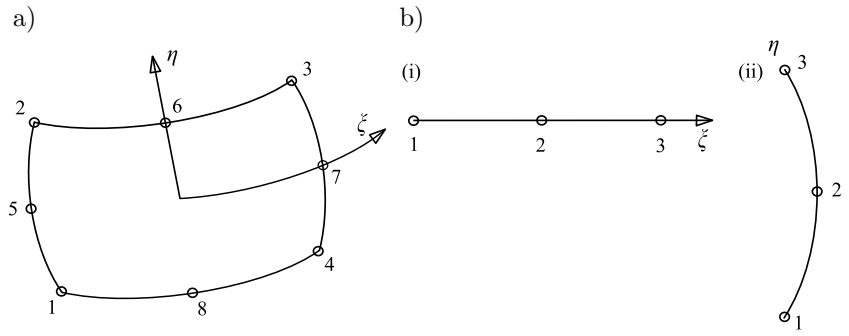

FIG. 3. a) Eight-noded shell element with isoparametric coordinates and b) three-noded stiffener elements, where: (i) X-stiffener, (ii) Y-stiffener.

where the shape functions derived from a cubic interpolation polynomial [27] are:

$$
\begin{aligned}
&N_i = (1+\xi\xi_i)(1+\eta\eta_i)(\xi\xi_i+\eta\eta_i-1)/4 && \text{for} \quad i=1,2,3,4,\\
&N_i = (1+\xi\xi_i)(1-\eta^2)/2, && \text{for} \quad i=5,7,\\
&N_i = (1+\eta\eta_i)(1-\xi^2)/2, && \text{for} \quad i=6,8.
\end{aligned} \tag{2.5}
$$

The generalized displacement vector of an element is expressed in terms of the shape functions and nodal degrees of freedom as:

$$[u] = [N]\,\{d_e\}\,, \tag{2.6}$$

i.e.,

$$\{u\} = \begin{Bmatrix} u \\ v \\ w \\ \alpha \\ \beta \end{Bmatrix} = \sum_{i=1}^{8} \begin{bmatrix} N_i & & & & \\ & N_i & & & \\ & & N_i & & \\ & & & N_i & \\ & & & & N_i \end{bmatrix} \begin{Bmatrix} u_i \\ v_i \\ w_i \\ \alpha_i \\ \beta_i \end{Bmatrix}.$$

The strain-displacement relation is given by

$$\{\varepsilon\} = [B]\,\{d_e\}\,,$$

where

$$[B] = \sum_{i=1}^{8} \begin{bmatrix} N_{i,x} & 0 & 0 & 0 & 0 \\ 0 & N_{i,y} & -\dfrac{N_i}{R_y} & 0 & 0 \\ N_{i,y} & N_{i,x} & 0 & 0 & 0 \\ 0 & 0 & 0 & N_{i,x} & 0 \\ 0 & 0 & 0 & 0 & N_{i,y} \\ 0 & 0 & 0 & N_{i,y} & N_{i,x} \\ 0 & 0 & N_{i,x} & N_i & 0 \\ 0 & 0 & N_{i,y} & 0 & N_i \end{bmatrix}.$$

The element stiffness matrix is thus written as:

$$[K_e] = \iint [B]^{\mathrm{T}}\,[E]\,[B]\,\mathrm{d}x\,\mathrm{d}y. \tag{2.7}$$

The element mass matrix is obtained from the integral

$$[M_e] = \iint [N]^{\mathrm{T}}\,[P]\,[N]\,\mathrm{d}x\,\mathrm{d}y, \tag{2.8}$$

where

$$[N] = \sum_{i=1}^{8} \begin{bmatrix} N_i & 0 & 0 & 0 & 0 \\ 0 & N_i & 0 & 0 & 0 \\ 0 & 0 & N_i & 0 & 0 \\ 0 & 0 & 0 & N_i & 0 \\ 0 & 0 & 0 & 0 & N_i \end{bmatrix}, \quad [P] = \sum_{i=1}^{8} \begin{bmatrix} P & 0 & 0 & 0 & 0 \\ 0 & P & 0 & 0 & 0 \\ 0 & 0 & P & 0 & 0 \\ 0 & 0 & 0 & I & 0 \\ 0 & 0 & 0 & 0 & I \end{bmatrix},$$

in which

$$P = \sum_{k=1}^{np} \int_{z_{k-1}}^{z_k} \rho \, \mathrm{d}z$$

and

$$I = \sum_{k=1}^{np} \int_{z_{k-1}}^{z_k} z\rho \, \mathrm{d}z.$$

For modeling the stiffeners, three-noded curved isoparametric beam elements (Fig. 3) are used. Stiffeners run only along the boundaries of the shell elements. In the stiffener element, each node has four degrees of freedom, i.e., u_{sx}, w_{sx}, α_{sx}, and β_{sx} for X-stiffener and v_{sy}, w_{sy}, α_{sy} and β_{sy} for Y-stiffener. The generalized force-displacement relation of stiffeners can be expressed as:

$$\begin{aligned} &X\text{-stiffener: } \{F_{sx}\} = [D_{sx}]\,\{\varepsilon_{sx}\} = [D_{sx}]\,[B_{sx}]\,\{\delta_{sxi}\}, \\ &Y\text{-stiffener: } \{F_{sy}\} = [D_{sy}]\,\{\varepsilon_{sy}\} = [D_{sy}]\,[B_{sy}]\,\{\delta_{syi}\}, \end{aligned} \tag{2.9}$$

where

$$\begin{aligned} \{F_{sx}\} &= \left[\; N_{sxx} \;\; M_{sxx} \;\; T_{sxx} \;\; Q_{sxxz} \;\right]^{\mathrm{T}}, \\ \{\varepsilon_{sx}\} &= \left[\; u_{sx.x} \;\; \alpha_{sx.x} \;\; \beta_{sx.x} \;\; (\alpha_{sx} + w_{sx.x}) \;\right]^{\mathrm{T}}, \\ \{F_{sy}\} &= \left[\; N_{syy} \;\; M_{syy} \;\; T_{syy} \;\; Q_{syyz} \;\right]^{\mathrm{T}}, \\ \{\varepsilon_{sy}\} &= \left[\; v_{sy.y} \;\; \beta_{sy.y} \;\; \alpha_{sy.y} \;\; (\beta_{sy} + w_{sy.y}) \;\right]^{\mathrm{T}}. \end{aligned}$$

The generalized displacements of the Y-stiffener and the shell are related by the transformation matrix $\{\delta_{syi}\} = [T]\,\{\delta\}$, where

$$[T] = \begin{bmatrix} 1 + \dfrac{e}{R_y} & \text{symmetric} & & \\ 0 & 1 & & \\ 0 & 0 & 1 & \\ 0 & 0 & 0 & 1 \end{bmatrix}.$$

This transformation is required due to the curvature of the Y-stiffener and $\{\delta\}$ is the appropriate portion of the displacement vector of the shell, excluding the displacement component along the x-axis.

Elasticity matrices are as follows:

$$[D_{sx}] = \begin{bmatrix} A_{11}b_{sx} & B'_{11}b_{sx} & B'_{12}b_{sx} & 0 \\ B'_{11}b_{sx} & D'_{11}b_{sx} & D'_{12}b_{sx} & 0 \\ B'_{12}b_{sx} & D'_{12}b_{sx} & \frac{1}{6}\left(Q_{44}+Q_{66}\right)d_{sx}b_{sx}^3 & 0 \\ 0 & 0 & 0 & b_{sx}S_{11} \end{bmatrix},$$

$$[D_{sy}] = \begin{bmatrix} A_{22}b_{sy} & B'_{22}b_{sy} & B'_{12}b_{sy} & 0 \\ B'_{22}b_{sy} & \frac{1}{6}(Q_{44}+Q_{66})b_{sy} & D'_{12}b_{sy} & 0 \\ B'_{12}b_{sy} & D'_{12}b_{sy} & D'_{11}d_{sy}b_{sy}^3 & 0 \\ 0 & 0 & 0 & b_{sy}S_{22} \end{bmatrix}, \tag{2.10}$$

where $D'_{ij} = D_{ij} + 2eB_{ij} + e^2A_{ij}$, $B'_{ij} = B_{ij} + eA_{ij}$, and A_{ij}, B_{ij}, D_{ij}, and S_{ij} are explained in [27]. Here the shear correction factor is taken as 5/6. In order to maintain compatibility between the shell and beam elements, the stiffener nodal degrees of freedom are to be transformed to shell degrees of freedom considering the eccentricity and curvature of the stiffener. The sectional parameters are calculated with respect to the mid-surface of the shell by which the effect of eccentricities of stiffeners is automatically included. The element stiffness matrices are of the following forms:

$$\begin{aligned} &\text{for } X\text{-stiffener: } [K_{xe}] = \int [B_{sx}]^{\mathrm{T}} [D_{sx}] [B_{sx}] \, \mathrm{d}x, \\ &\text{for } Y\text{-stiffener: } [K_{ye}] = \int [B_{sy}]^{\mathrm{T}} [D_{sy}] [B_{sy}] \, \mathrm{d}y. \end{aligned} \tag{2.11}$$

The integrals are converted to isoparametric coordinates and are carried out by 2-point Gauss quadrature method. Finally, the element stiffness matrix of the stiffened shell is obtained by appropriate matching of the nodes of the stiffener and shell elements through the connectivity matrix and is given as:

$$[K_e] = [K_{she}] + [K_{xe}] + [K_{ye}]. \tag{2.12}$$

The element stiffness matrices are assembled to get the global matrices.

The element mass matrix for the stiffener element is written as:

$$\begin{aligned} &\text{for } X\text{-stiffener: } [M_{sx}] = \iint [N]^{\mathrm{T}} [P] [N] \, \mathrm{d}x, \\ &\text{for } Y\text{-stiffener: } [M_{sy}] = \iint [N]^{\mathrm{T}} [P] [N] \, \mathrm{d}y. \end{aligned} \tag{2.13}$$

Here $[N]$ is a 3×3 diagonal matrix.

$$\text{for } X\text{-stiffener: } [P] = \sum_{i=1}^{3} \begin{bmatrix} \rho b_{sx} d_{sx} & 0 & 0 & 0 \\ 0 & \rho b_{sx} d_{sx} & 0 & 0 \\ 0 & 0 & \dfrac{\rho b_{sx} d_{sx}^2}{12} & 0 \\ 0 & 0 & 0 & \dfrac{\rho (b_{sx} d_{sx}^3 + b_{sx}^3 d_{sx})}{12} \end{bmatrix},$$

$$\text{for } Y\text{-stiffener: } [P] = \sum_{i=1}^{3} \begin{bmatrix} \rho b_{sy} d_{sy} & 0 & 0 & 0 \\ 0 & \rho b_{sy} d_{sy} & 0 & 0 \\ 0 & 0 & \dfrac{\rho b_{sy} d_{sy}^2}{12} & 0 \\ 0 & 0 & 0 & \dfrac{\rho (b_{sy} d_{sy}^3 + b_{sy}^3 d_{sy})}{12} \end{bmatrix}.$$

The mass matrix of the stiffened shell element is the sum of the matrices of the shell and the stiffeners matched at the appropriate nodes.

$$[M_e] = [M_{she}] + [M_{xe}] + [M_{ye}]. \tag{2.14}$$

The element mass matrices are assembled to get the global matrices.

The finite element code developed here takes the position and size of the cutout as input. The program is capable of generating non uniform finite element mesh all over the shell surface. So the element size is gradually decreased near the cutout margins. Such finite element mesh is redefined in steps and a particular grid is chosen to obtain the fundamental frequency when the result does not improve by more than one percent on further refining. Convergence of results is ensured in all the problems considered here.

2.3. Equations of motion

For the present case, the dynamic form of the principle of virtual work can be represented as:

$$0 = \int_{\Omega} \big[N_1\delta\varepsilon_1^0 + N_2\delta\varepsilon_2^0 + N_6\delta\varepsilon_6^0 + M_1\delta\kappa_1 + M_2\delta\kappa_2 + M_6\delta\kappa_6 + Q_1\delta\varepsilon_5^0 + Q_2\delta\varepsilon_4^0 + (P_1\,\ddot{u} + P_2\ddot{\alpha})\,\delta u + \left(P_1\,\ddot{v} + P_2\ddot{\beta}\right)\delta v + I_1\ddot{w}\delta w + (I_3\ddot{\alpha} + P_2\ddot{u})\,\delta\alpha + \left(I_3\ddot{\alpha} + \overline{P}_2\ddot{v}\right)\big]\theta_1\theta_2\,\mathrm{d}\xi\,\mathrm{d}\eta. \tag{2.15}$$

The governing equations of motion are obtained from Eq. (2.15) by carrying out integration by parts of the displacement gradients in ε_i. Thus it yields:

$$[K\,\{\Delta\}] + \left[M\left\{\ddot{\Delta}\right\}\right] = 0, \tag{2.16}$$

where $\{\Delta\} = \{\{u\},\{v\},\{w\},\{\alpha\},\{\beta\}\}^{\mathrm{T}}$, $[K]$ is the element stiffness matrix and $[M]$ is the element mass matrix. In the case of the eight-node quadratic element, the size of the element stiffness matrix is 40×40. Its evaluation requires numerical integration. A reduced integration technique is employed to obtain the coefficients dealing with the shear energy terms in order to avoid any locking effect.

For undamped free vibration study, assembly of the elemental Eq. (2.16) yields the following eigenvalue form with $\Delta(t) = \Delta e^{i\omega t}$:

$$\left([K] - \omega^2\,[M]\right)\{\Delta\} = 0, \tag{2.17}$$

where ω is the circular frequency and Δ denotes the mode shape. This is a generalized eigenvalue problem and is solved by the subspace iteration algorithm with proper consideration of the boundary conditions.

3. Validation study and numerical examples

In order to ascertain the validity of the stiffener formulation, the natural frequency of a square plate with clamped edges and central stiffeners is computed and compared with the literature values [28, 29]. The plate dimensions are: length = breadth = 0.2032 m, the thickness of shell = 0.0013716 m, depth of stiffener = 0.00635 m, the stiffener is placed eccentrically at the bottom, the material property is $E = 6.87 \cdot 10^{10}$ N/m^2, and $\nu = 0.29$, $\rho = 2823$ kg/m^3. The comparison shown in Table 1 reveals a good agreement of the results from

Table 1. Natural frequency in Hz for the clamped square plate with central stiffener.

Mode no.	Ref. [28]	Ref. [29]		Present model
		N8(FEM)	N9(FEM)	
1	711.8	725.2	725.1	733

the present method with earlier ones. Thus, the stiffener formulation is implemented adequately in the present model.

Next, the suitability of cut-out formulation is determined by comparing the fundamental frequency of a cut-out borne cylindrical shell of $(0/90)_4$ lamination for the following support conditions, viz., corner point supported, simply supported, and clamped. The geometric properties considered are: $a/b = 1$, $a/h = 100$, $a'/b' = 1$, $h/R_x = 0$, $h/R_y = 1/300$. Table 2 presents the fundamental frequencies calculated by the present method and benchmark results [30]. The results agree well with each other. Thus it can be ascertained that the cut-out formulation is correctly implemented in the present method. The fundamental frequency is taken to be converged for a particular finite element grid if further refinement of the grid does not yield a change in result by more than 0.1%. With this criterion, a 10×10 mesh is found to be appropriate. With eight-noded curved quadratic isoparametric elements having five degrees of freedom at each node, the total number of degrees of freedom ranges between 1381 and 1571, depending on the boundary conditions considered here. Thereby, the present FE model is capable of tackling the vibration behavior of cut-out borne stiffened cylindrical shells successfully.

Table 2. Fundamental frequency ($\overline{\omega}$) for the cut-out borne composite cylindrical shell.

a'/a	Ref. [30]	Present model		
		8×8	10×10	12×12
Corner point supported				
0.0	11.486	11.339	11.336	11.352
0.1	11.679	11.375	11.371	11.349
0.2	11.708	11.367	11.338	11.354
0.3	11.688	11.342	11.368	11.382
0.4	11.684	11.363	11.345	11.394
Simply supported				
0.0	26.990	26.991	26.995	27.004
0.1	27.042	27.034	27.005	27.001
0.2	27.291	27.263	27.258	27.251
0.3	27.913	27.897	27.876	27.861
0.4	28.711	28.686	28.667	28.637
Clamped				
0.0	69.360	69.156	69.016	68.979
0.1	68.776	69.044	68.659	68.439
0.2	64.751	64.569	64.232	64.065
0.3	59.317	59.282	58.829	58.819
0.4	59.303	59.568	59.107	59.180

An anti-symmetric angle-ply cylindrical shell panel (Fig. 2) is taken up for further analysis to consider vibration behavior at higher modes for different parametric variations. The cut-out imperfection is considered to be located concentric on the shell, and stiffeners run along the edges of perforation and extend to the edge of the shell. The material chosen has the following properties: $E_{11}/E_{22} = 25$, $G_{23} = 0.2E_{22}$, $G_{13} = G = 0.5E_{22}$, $\nu_{12} = \nu_{21} = 0.25$, and $\rho = 100$. The geometric properties considered are: $a/b = 1$, $a/h = 100$, $a'/b' = 1$, $h/R_x = 0$, $h/R_y = 1/300$. The width of the stiffener is the same as the shell thickness h in all cases. The ratio of stiffener depth to shell thickness (d_{st}/h) is taken as 2 unless stated otherwise. Single-layer stiffener has ply orientated along the length direction of the stiffeners.

Anti-symmetric angle-ply stacking sequences are considered with $(\theta/-\theta)_n$, where n is the number of layers, and fiber orientation angle θ varies as 0°, 15°, 30°, 45°, 60°, 75°, and 90°. Numerical experimentation is carried out to observe the effect of the degree of orthotropy ($E_{11}/E_{22} = 5$, 10, 20, 25, 30, 40 and 50), and width/thickness ratio ($b/h = 10$, 20, 50, 100) on non-dimensional natural frequencies $[\overline{\omega} = \omega\, a^2 \left(\rho/E_{22}h^2\right)^{1/2}]$. For the present numerical study, six different boundary conditions are taken up: CSCS, CSSC, FCCF, FCFC, FSFS, and FSSF. Here, C stands for clamped, S stands for simply supported, and F stands for free boundary. The four boundaries are designated in counter-clockwise order starting from the boundary $x = 0$. For example, the CSCS boundary implies that the shell is clamped along $x = 0$, simply supported along $y = 0$, clamped along $x = a$, and simply supported along $y = b$. A schematic representation of the arrangement of boundary conditions is given in Fig. 4.

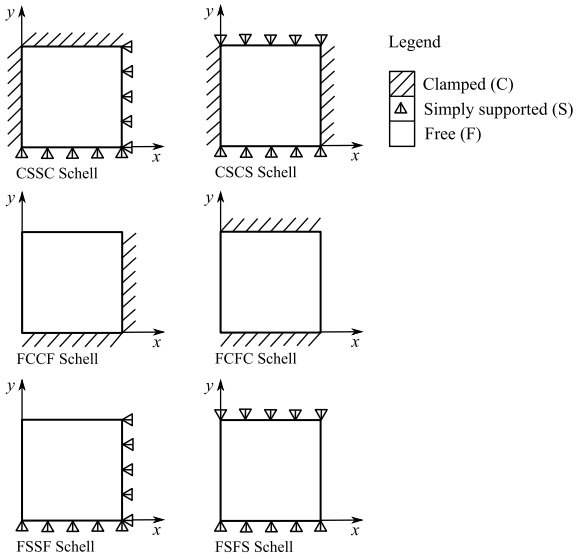

FIG. 4. Arrangement of boundary conditions.

4. Results and discussion

Non-dimensional fundamental frequencies (first-mode) of shells with cut-out for 2, 4, and 10-layered cases are presented in Table 3. A column-wise highest value of frequency is marked with an asterisk. For all the cases considered here, it is evident that the fundamental frequency increases as the number of boundary constraints increases. Thus, the performance of CSCS and CSSC shells is better than FCCF and FCFC shells, followed by FSFS and FSSF shells. The results vary the most for the FCFC boundary condition. It can also be noted that the maximum frequency values for each boundary condition occur at 10-layer

Table 3. Non-dimensional fundamental frequency of multi-layered shell with cut-out.

Angle of ply [°]	Boundary condition	2-layer	4-layer	10-layer
0	CSCS	5.477	5.477	5.477
15		6.747	7.583	7.743
30		6.561	8.737	9.231
45		7.048*	9.011*	9.453*
60		6.787	8.293	8.647
75		5.695	6.717	6.966
90		6.032	6.032	6.032
0	CSSC	6.998	6.998	6.999
15		7.351*	8.695	8.940
30		6.980	8.976*	9.376*
45		7.048	8.847	9.213
60		6.475	7.797	8.056
75		5.035	5.900	6.966
90		4.898	4.898	4.898
0	FCCF	2.382	2.380	2.383
15		2.441	2.819	2.900
30		2.707	3.410	3.552
45		3.052	3.919	4.102
60		3.216*	4.157*	4.371*
75		2.960	3.382	3.473
90		2.848	2.848	2.848
0	FCFC	13.450*	13.451*	13.451*
15		8.847	11.873	12.571
30		6.468	9.465	10.123
45		4.706	6.574	6.998
60		3.460	4.127	4.291
75		2.946	3.007	3.022
90		2.874	2.874	2.874

Table 3. [Cont.].

Angle of ply [°]	Boundary condition	2-layer	4-layer	10-layer
0	FSFS	4.469	4.469	4.469
15		4.710*	5.173	5.263
30		4.452	5.688*	5.770*
45		3.321	4.602	4.892
60		2.504	2.966	3.078
75		2.124	2.174	4.469
90		2.017	2.017	2.017
0	FSSF	2.116	2.116	2.117
15		2.178	2.508	2.578
30		2.421	3.081	3.210
45		2.688	3.521	3.692
60		2.853*	3.583*	3.736*
75		2.469	2.811	2.882
90		2.230	2.230	2.230

laminates. As the 10-layer laminate is found to exhibit the best performance in terms of fundamental frequency, subsequent studies concentrate on these laminates only.

4.1. Role of fiber orientation

The fiber orientation angle of 10-layer anti-symmetric angle ply laminate is varied as 0°, 15°, 30°, 45°, 60°, 75°, and 90°, keeping total thickness and layers the same. Variation of the non-dimensional natural frequency with boundary conditions and lamination angles is plotted in Fig. 5. Seven stacking sequences for anti-symmetric angle-ply laminations are considered: $(0/-0)_{10}$, $(15/-15)_{10}$, $(30/-30)_{10}$, $(45/-45)_{10}$, $(60/-60)_{10}$, $(75/-75)_{10}$, and $(90/-90)_{10}$ with six different boundary conditions for the shell edges, viz., CSCS, CSSC, FCCF, FCFC, FSFS, and FSSF.

In the case of CSCS and FSSF shells, for the 1st, 2nd, 3rd, 4th, and 5th mode, the non-dimensional frequency has an increasing trend with fiber orientation angle varying from 0° to 45°. In the case of CSSC and FSFS shells, natural frequency increases with fiber orientation angle increasing from 0° to 30°. When the lamination angle is increased further, natural frequencies decrease. Similarly, for FCCF shells, the natural frequency increases with a fiber orientation angle up to 60°, whereas the natural frequencies of FCFC shells decrease as the fiber orientation angle increases. The lamination angle and boundary conditions interrelate in a complex way; hence, no unified trend can be observed. Frequencies depend on three contributions: extensional stiffness, bending stiff-

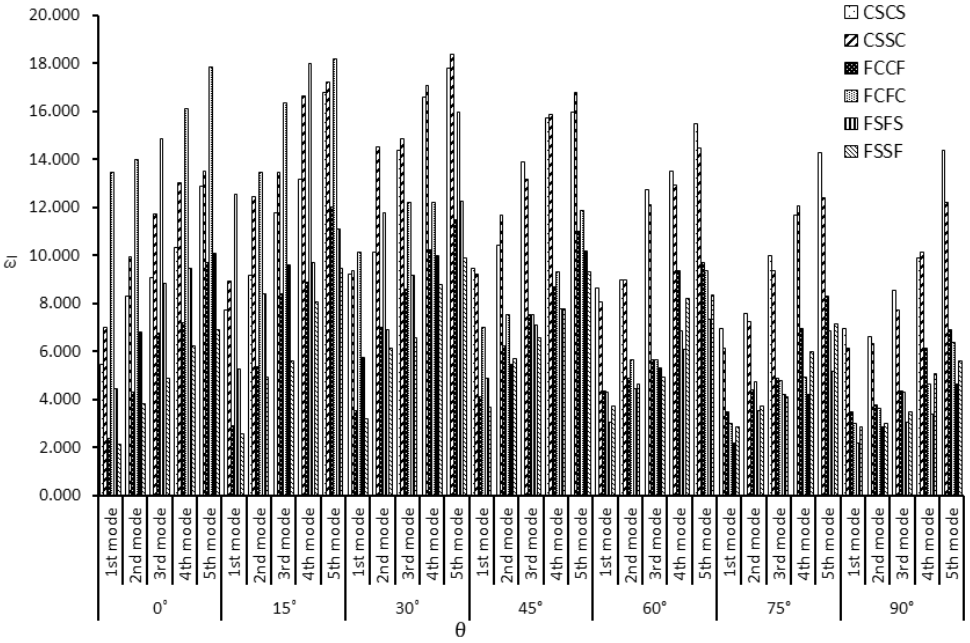

FIG. 5. Variation of non-dimensional fundamental frequency with the fiber orientation angle.

ness, and bending-stretching coupling stiffness. These factors depend on shell geometry, lamination and boundary conditions. For different laminations and edge conditions taken up here, natural frequency has increasing nature from the first to fifth mode significantly, barring a few cases where the difference in frequency parameter of two consecutive modes is insignificant. However, for different lamination angles taken up here, the performance of CSSC and FCFC shells is better than CSCS, FCCF, and FSFS shells, followed by the FSSF shell. Thus, not only the number of boundary constraints but also the arrangement of boundary constraints play an important role in free vibration performance.

4.2. Role of material anisotropy

Variation in material anisotropy affects the frequencies of 10-layer anti-symmetric angle-ply shells with cut-out, and the results are presented in Figs. 6–12 for varying fiber orientation angles (0°, 15°, 30°, 45°, 60°, 75°, and 90°) and boundary conditions (CSCS, CSSC, FCCF, FCFC, FSFS, and FSSF boundary conditions). The material properties are considered as $G_{12}/E_{22} = 0.5$, $\nu_{12} = 0.25$, and E_{11}/E_{22} ratio is varied as 5, 10, 20, 25, 30, 40, 50. As can be observed in these figures, the 1st, 2nd, 3rd, 4th, and 5th mode frequency parameter increases monotonically with the degree of orthotropy for different laminations and boundaries considered here.

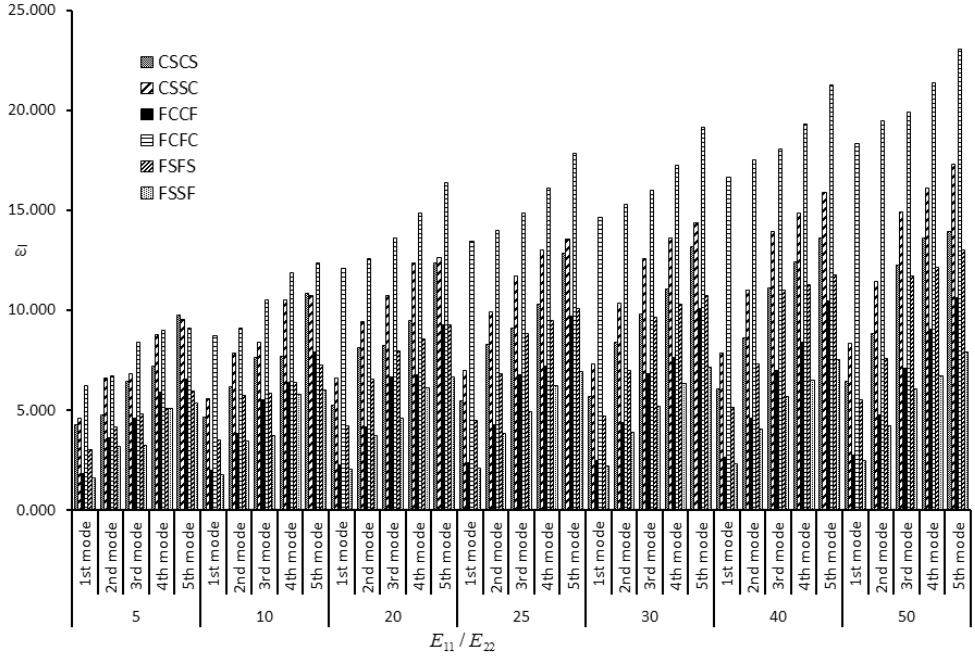

FIG. 6. Variation of non-dimensional fundamental frequency with material anisotropy for $(0/-0)_{10}$ lamination.

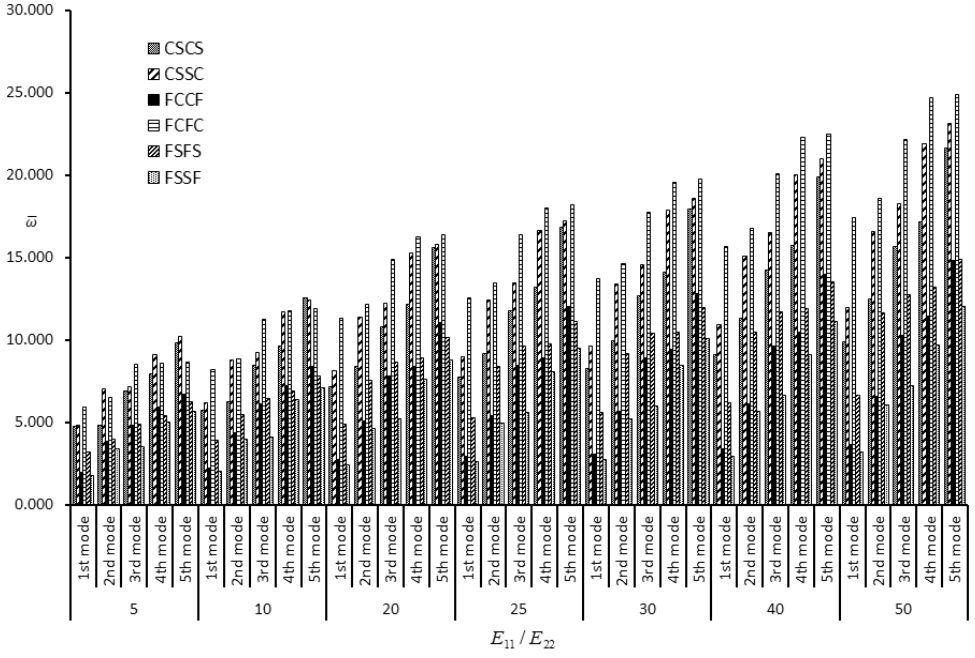

FIG. 7. Variation of non-dimensional fundamental frequency with material anisotropy for $(15/-15)_{10}$ lamination.

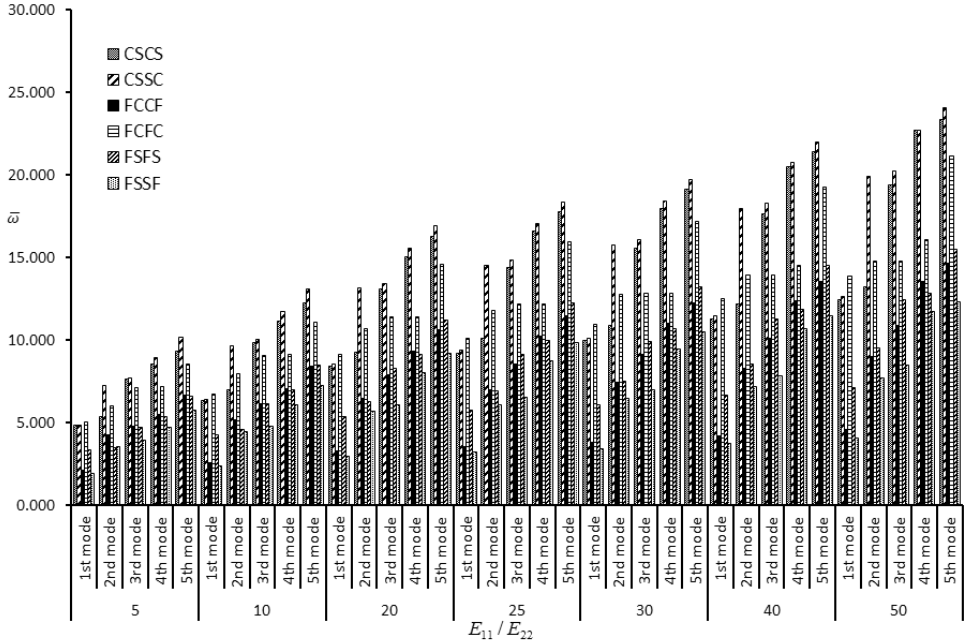

FIG. 8. Variation of non-dimensional fundamental frequency with material anisotropy for $(30/-30)_{10}$ lamination.

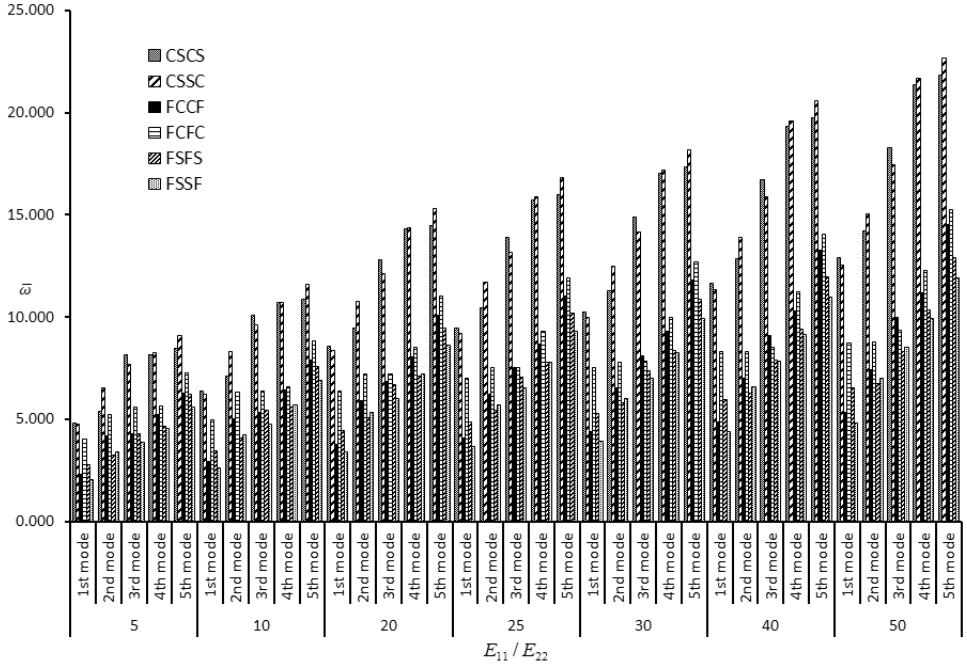

FIG. 9. Variation of non-dimensional fundamental frequency with material anisotropy for $(45/-45)_{10}$ lamination.

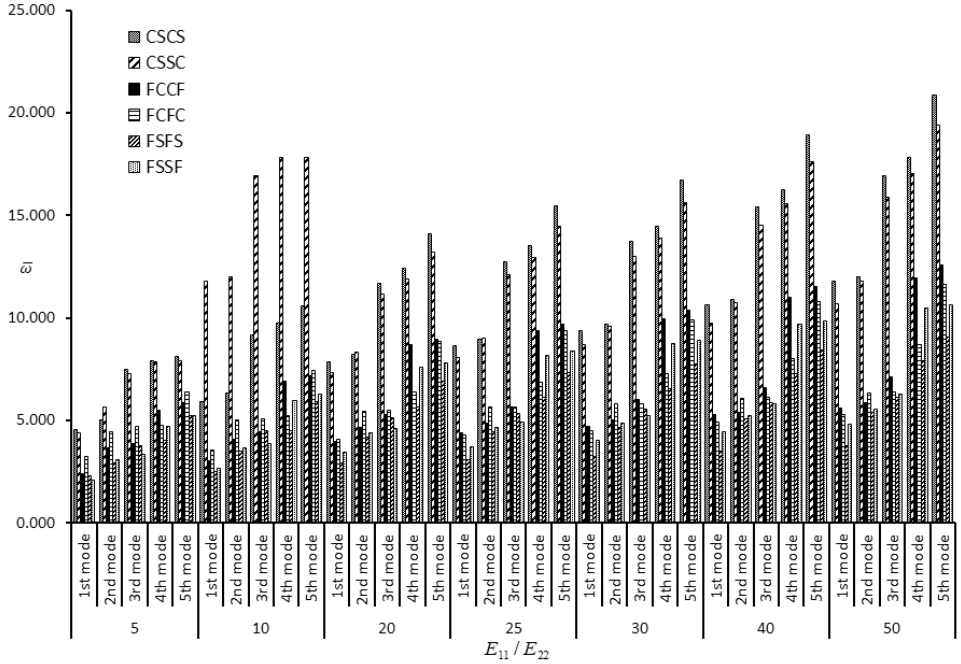

FIG. 10. Variation of non-dimensional fundamental frequency with material anisotropy for $(60/-60)_{10}$ lamination.

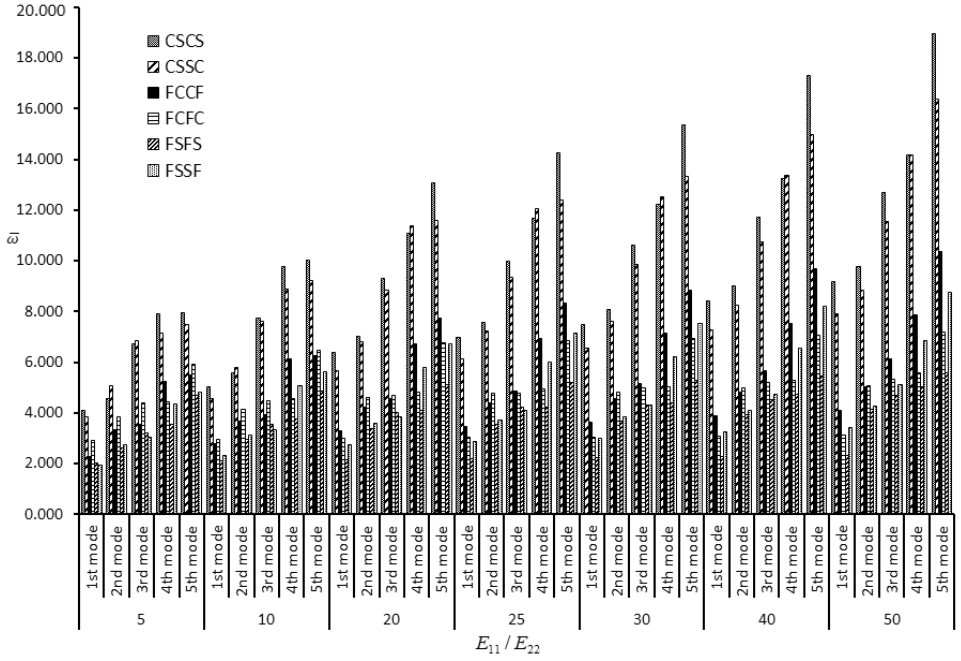

FIG. 11. Variation of non-dimensional fundamental frequency with material anisotropy for $(75/-75)_{10}$ lamination.

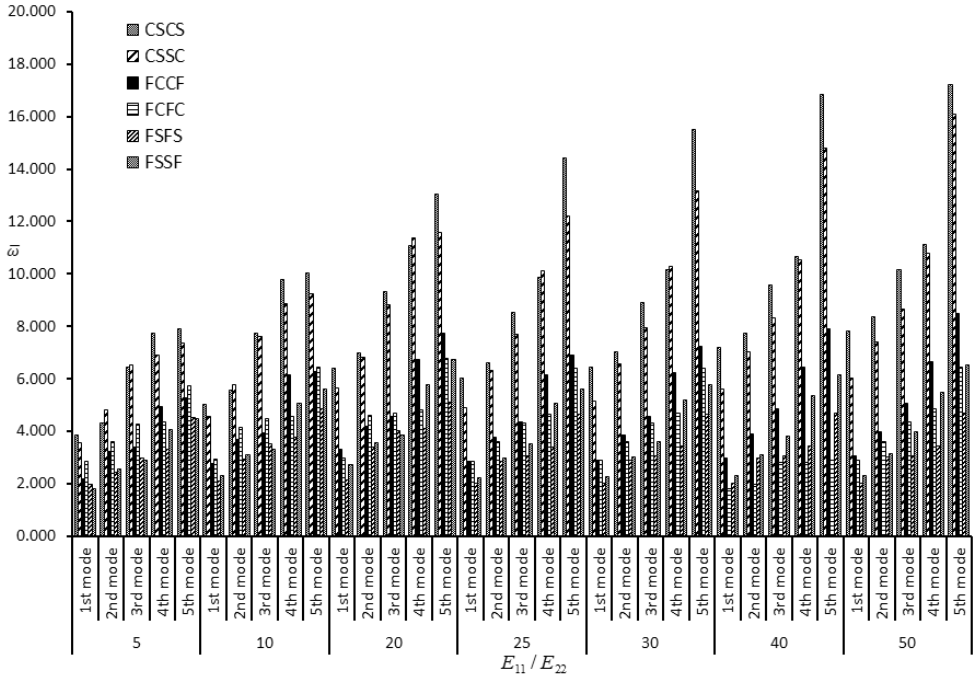

FIG. 12. Variation of non-dimensional fundamental frequency with material anisotropy for $(90/-90)_{10}$ lamination.

In Figs. 6–12, it is clearly observed that the change in frequency due to material anisotropy is very pronounced in shells with CSCS and CSSC boundary conditions. With the increase in lamination angle, the effect of anisotropy is more pronounced. The effect of anisotropy in FCFC shell is also prominent for lower lamination angles. At higher lamination angles, the effect of anisotropy is not so significant. But the frequency parameters at each lamination angle increase with the increase in E_{11}/E_{22} ratio from the 1st mode to the 5th mode, except very few cases. In Fig. 8, it is observed that CSCS shells yield the maximum value of natural frequency at $E_{11}/E_{22} = 10$. In all other cases, the values of non-dimensional frequency would reach their maximum value at $E_{11}/E_{22} = 50$. The variations are clearly visible in the case of CSCS, CSSC and FCFC shells. Such an increase in frequencies is not so significant in the case of FCCF, FSFS and FSSF shells. For very few cases, it is observed that the frequency does not alter much for consecutive modes.

4.3. Role of width-to-thickness ratio

For a 10-layer laminate with constant width, an increase in width/thickness ratio means a decrease in the thickness of the shell. Figures 13–19 show the

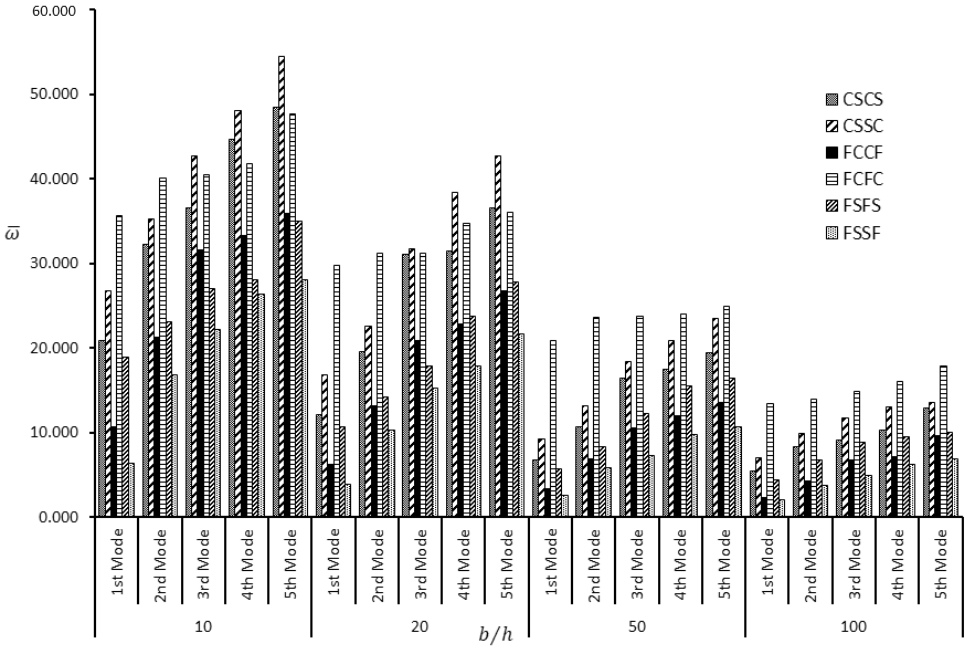

FIG. 13. Variation of non-dimensional fundamental frequency with b/h ratio for $(0/-0)_{10}$ lamination.

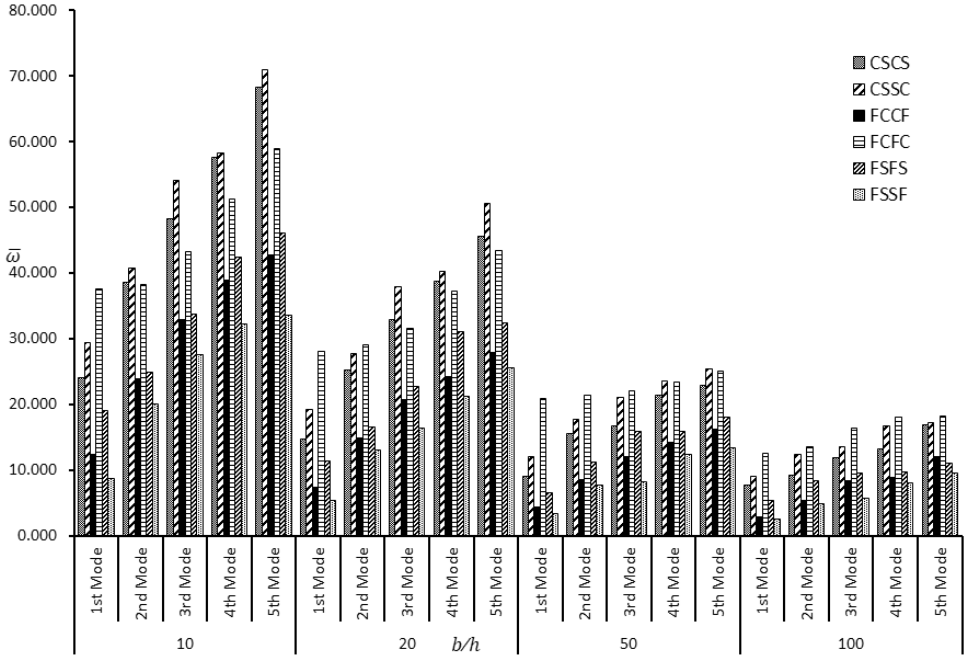

FIG. 14. Variation of non-dimensional fundamental frequency with b/h ratio for $(15/-15)_{10}$ lamination.

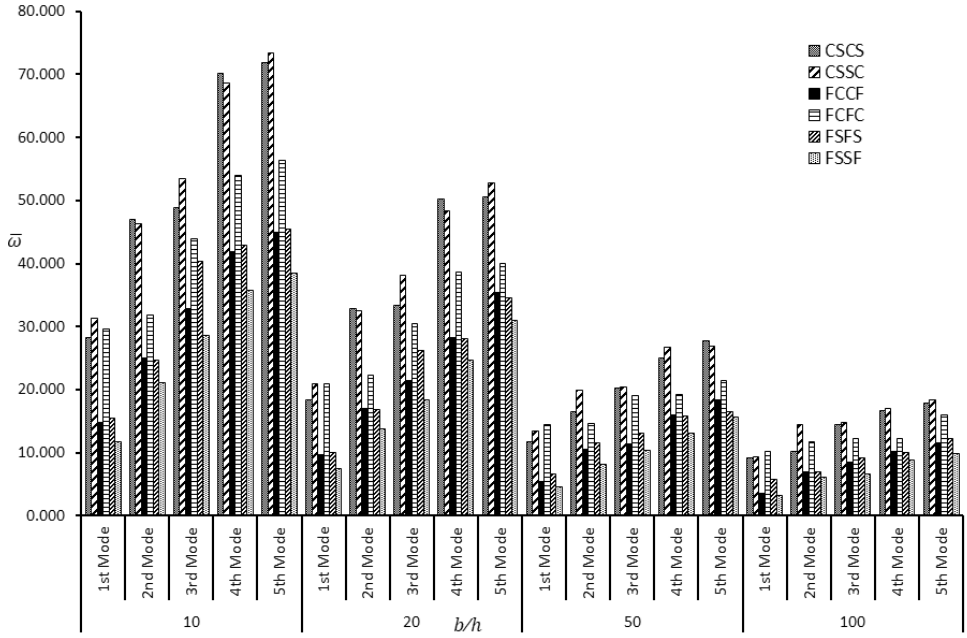

FIG. 15. Variation of non-dimensional fundamental frequency with b/h ratio for $(30/-30)_{10}$ lamination.

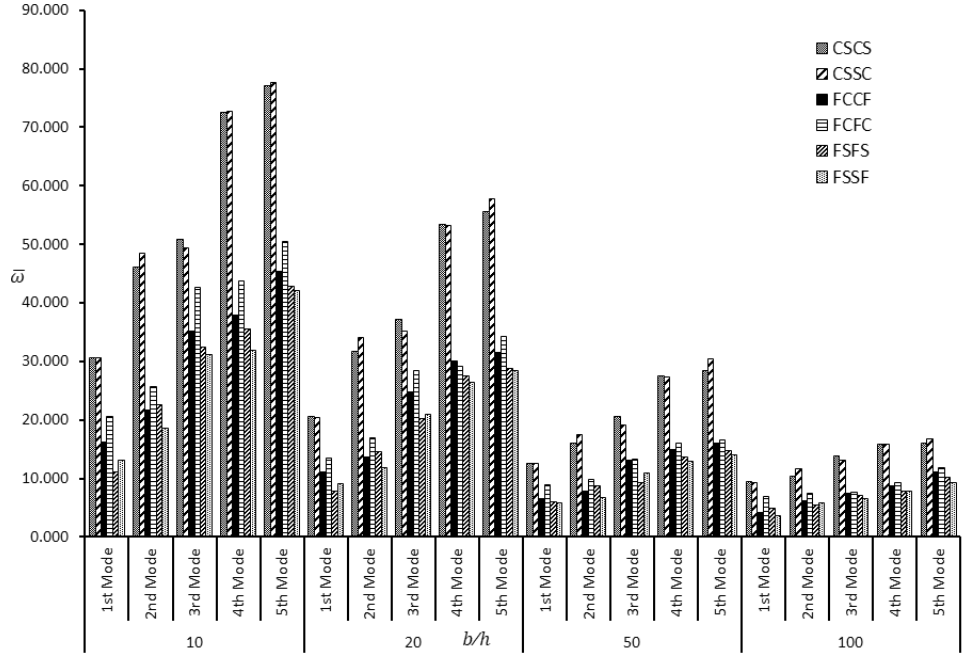

FIG. 16. Variation of non-dimensional fundamental frequency with b/h ratio for $(45/-45)_{10}$ lamination.

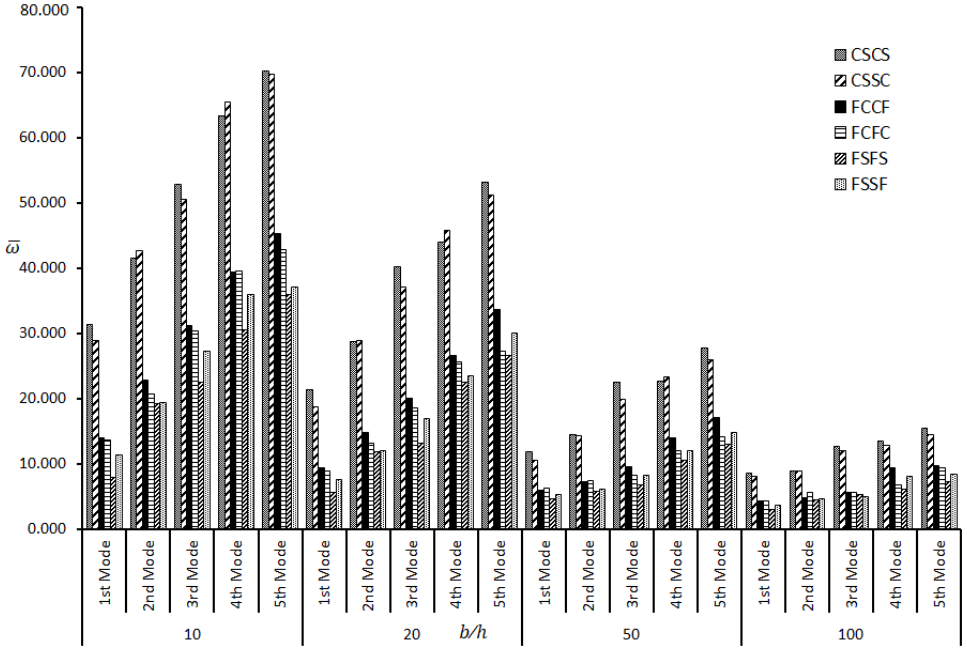

FIG. 17. Variation of non-dimensional fundamental frequency with b/h ratio for $(60/-60)_{10}$ lamination.

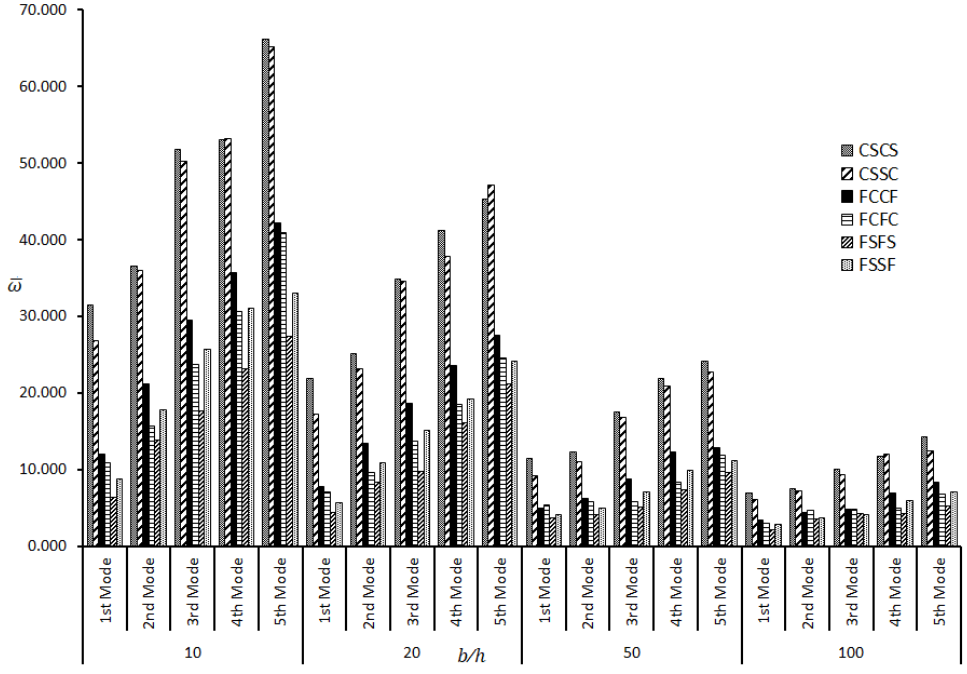

FIG. 18. Variation of non-dimensional fundamental frequency with b/h ratio for $(75/-75)_{10}$ lamination.

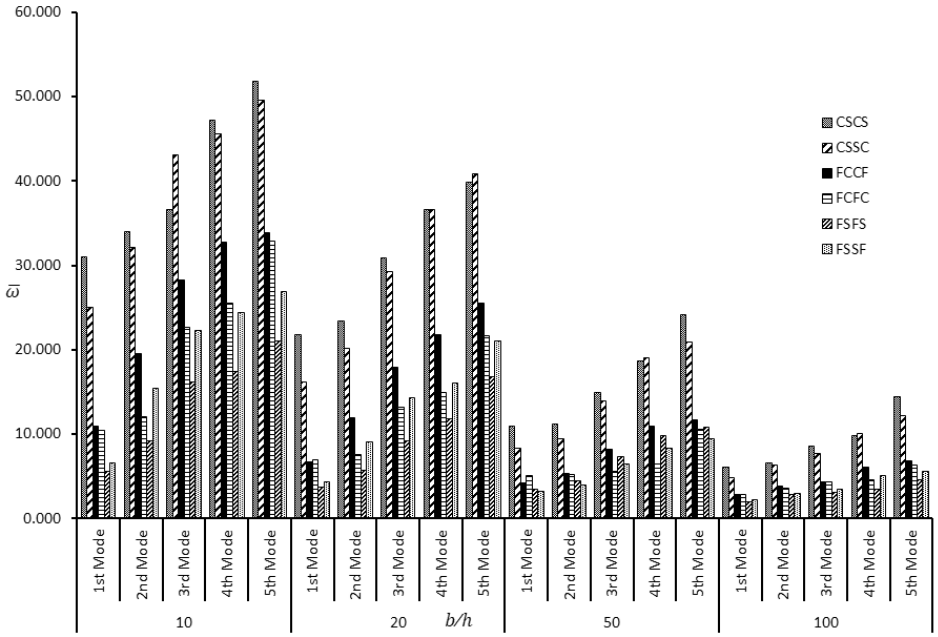

FIG. 19. Variation of non-dimensional fundamental frequency with b/h ratio for $(90/-90)_{10}$ lamination.

variation of frequency for the 1st, 2nd, 3rd, 4th, and 5th mode with change in width/thickness ratios and edge supports for varying lamination angles (0°, 15°, 30°, 45°, 60°, 75°, and 90°). Ten-layer anti-symmetric angle-ply laminates with changing width/thickness ratios ($b/h = 10, 20, 50, 100$) are analyzed. It is clearly seen in the figures that the values of frequency decrease with the increase of the width-thickness ratio. It is obvious that due to the increase in thickness stiffness of the shell increases. A significant decrease in frequency is observed for CSCS, CSSC, FCFC, and FCCF shells with higher values of the width/thickness ratio. But for FSSF and FSFS shells, the change in frequency due to change in width-to-thickness ratios is not so significant. For a thick shell, when two opposite edges or two adjacent edges are clamped, due to increased stiffness of the shell frequency increases significantly. But when the thickness of the shell decreases, stiffness decreases significantly. So the effect of shell thickness on free vibration response is more pronounced than the number of support constraints in the case of shells with a greater number of edge constraints. A similar trend is observed for higher modes as well.

4.4. Mode shapes

The typical mode shapes corresponding to the first five modes of vibration for $(60/-60)_{10}$ lamination and central cut-out with size 0.2 are plotted in Fig. 20

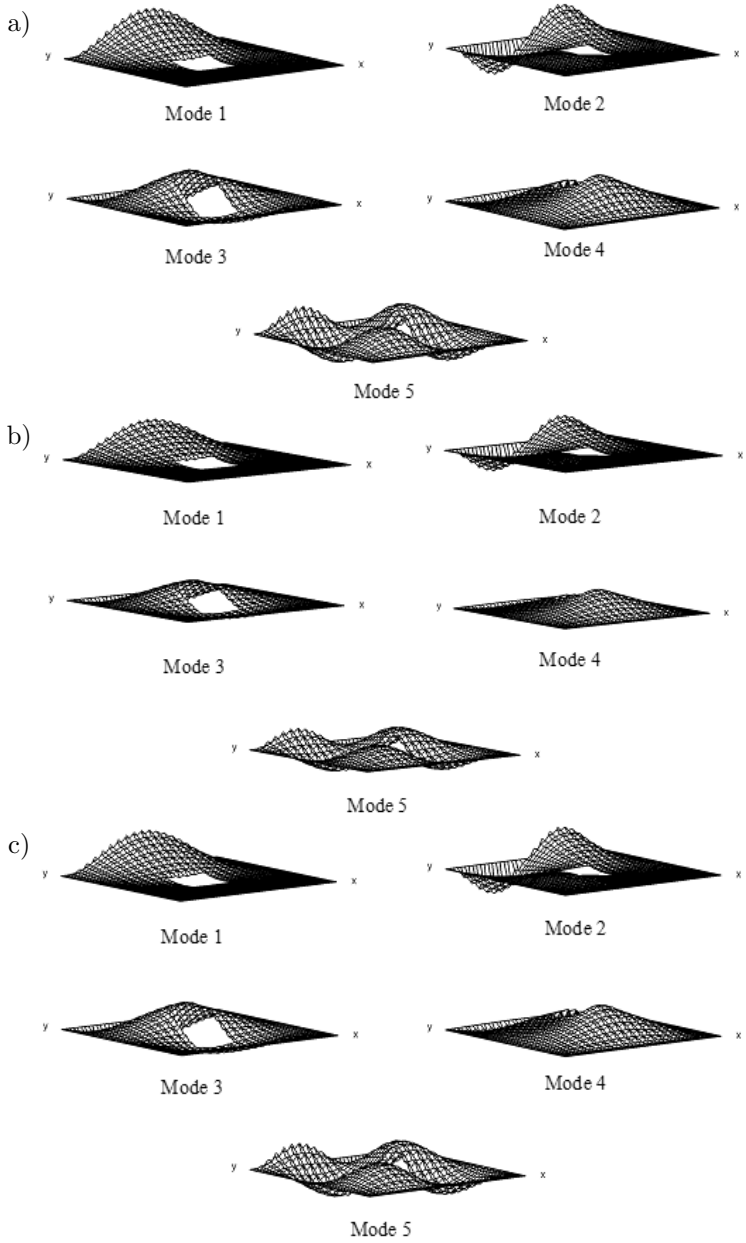

FIG. 20. Typical mode shapes corresponding to $(60/-60)_{10}$ laminated shell with central cut-out for the CSCS boundary condition for the first five modes: a) $E_{11}/E_{22} = 10$, b) $E_{11}/E_{22} = 25$, c) $E_{11}/E_{22} = 40$.

for three different values of degree of orthotropy. The boundary condition considered here is CSCS and b/h is 100. The normalized displacements are drawn with the shell mid-surface as the reference. Mode shapes get complicated with

an increase in mode number as a combination of bending and torsional modes are present. The positions of crests and troughs also change with the mode number. It can be seen in these plots that the mode shapes do not alter significantly with the variation of orthotropy features. Details of mode shapes for other shell configurations are omitted for brevity. For other laminations, boundary conditions, degree of orthotropy, width-to-thickness ratios and cut-out sizes, the mode shapes do not change to an appreciable amount.

4.5. Comparison with other shell forms

It remains interesting to see if the foregoing results and variations are specific to cylindrical shells or hold good for cut-out borne shell of any geometry. To explore it, a comparison of the present results with those for anti-symmetric angle-ply laminated composite hypar shells (hyperbolic paraboloid bounded by straight edges) with cut-out [21] is attempted. It was reported for hypar shells that as the number of layers increases, the fundamental frequency increases. With the increase in lamination angle, the non-dimensional natural frequency may increase or decrease, but from the first mode to the fifth mode, natural frequency always increases or remains the same in very few cases. The first, second, third, fourth, and fifth non-dimensional frequency parameter increases monotonically with a degree of orthotropy for all the laminations and boundary conditions. With the increase in width-to-thickness ratios, frequencies decrease from the first mode to the fifth mode. In a nutshell, the free vibration behavior of hypar shells was found to primarily depend on the number of boundary constraints irrespective of other parametric variations in terms of fiber orientation angle, degree of orthotropy and width-to-thickness ratio. Thus by comparing the results from the present analysis with those reported earlier for hypar shells [21], it may be inferred that the mode-frequency behavior of cut-out borne stiffened composite shells do follow some similar trends, but the exact behavioral pattern depends on the shell geometry. No generalized pattern applicable for all types of shells, e.g., cylindrical, spherical, hypar, elliptic paraboloid, conoidal, etc., can be obtained. One has to treat each individual shell separately and perform a similar analysis to obtain the higher mode frequencies and their variation with change in different parametric conditions, including geometry, size, boundary conditions, laminations, degree of orthotropy, etc., for effective use of these shell form in the presence of cut-out. In the present study, the dynamic behavior of laminated composite stiffened cylindrical shell with cut-out is studied by considering the natural frequencies of the first five modes. For civil and architectural structures where such laminated cylindrical shells are commonly used, consideration of first few modes is sufficient. However, there is always scope for consideration of even higher frequencies.

5. Conclusions

Higher modes of vibration of the laminated stiffened cylindrical shell with cut-out were analyzed using the finite element method. Analyzing the results, the following can be concluded.

1) Fundamental frequency increases with an increase in layers.
2) If the fiber orientation angle increases, the non-dimensional fundamental frequency may increase or decrease depending on boundary conditions. The laminations and edge conditions interrelate in a complex fashion, and a uniform trend cannot be determined. This is because stiffness due to extension, bending, and bending-stretching coupling contribute to frequency. In turn, the frequency depends on shell geometry, lamination and edge conditions.
3) As the lamination angle increases, the effect of anisotropy is not so significant. But the frequency parameters under each lamination angle increase with the increase in E_{11}/E_{22} ratio from the 1st mode to 5th mode, except very few cases.
4) The effect of shell thickness on free vibration response is more pronounced than the number of edge constraints in shells with a higher number of edge constraints. A similar trend is observed for higher modes also.

Moreover, comparison with hypar shells reveals that although the mode-frequency behavior of cut-out borne stiffened composite shells follows somewhat similar trends, the exact behavioral pattern depends on the shell geometry.

References

1. Liew K.M., Lim C.W., Vibration of perforated doubly-curved shallow shells with rounded corners, *International Journal of Solids and Structures*, **31**(11): 1519–1536, 1994, doi: 10.1016/0020-7683(94)90012-4.

2. Liew K.M., Lim C.W., A global continuum Ritz formulation for flexural vibration of pretwisted trapezoidal plates with one edge built in, *Computer Methods in Applied Mechanics and Engineering*, **114**(3–4): 233–247, 1994, doi: 10.1016/0045-7825(94)90173-2.

3. Lim C.W., Liew K.M., A pb-2 Ritz formulation for flexural vibration of shallow cylindrical shells of rectangular planform, *Journal of Sound and Vibration*, **173**(3): 343–375, 1994, doi: 10.1006/jsvi.1994.1235.

4. Liew K.M., Lim C.W., Vibratory characteristics of cantilevered rectangular shallow shells of variable thickness, *AIAA Journal*, **32**(2): 387–396, 1994, doi: 10.2514/3.59996.

5. Lim C.W., Liew K.M., Vibration of pretwisted cantilever trapezoidal symmetric laminates, *Acta Mechanica*, **111**(3): 193–208, 1995, doi: 10.1007/BF01376930.

6. Liew K.M., Lim C.W., Kitipornchai S., Vibration of shallow shells: a review with bibliography, *Applied Mechanics Reviews*, **50**(8): 431–444, 1997, doi: 10.1115/1.3101731.

7. Sivasubramonian B., Kulkarni A.M., Rao G.V., Krishnan A., Free vibration of curved panels with cutouts, *Journal of Sound and Vibration*, **200**(2): 227–234, 1997, doi: 10.1006/jsvi.1996.0637.

8. Sivasubramonian B., Rao G.V., Krishnan A., Free vibration of longitudinally stiffened curved panels with cutout, *Journal of Sound and Vibration*, **226**(1): 41–55, 1999, doi: 10.1006/jsvi.1999.2281.

9. Sai Ram K.S., Sreedhar Babu T., Free vibration of composite spherical shell cap with and without a cutout, *Computers & Structures*, **80**(23): 1749–1756, 2002, doi: 10.1006/S0045-7949(02)00210-9.

10. Hota S.S., Chakravorty D., Free vibration of stiffened conoidal shell roofs with cutouts, *Journal of Vibration and Control*, **13**(3): 221–240, 2007, doi: 10.1177/1077546307072353.

11. Hota S.S., Padhi P., Vibration of plates with arbitrary shapes of cutouts, *Journal of Sound and Vibration*, **302**(4–5): 1030–1036, 2007, doi: 10.1016/j.jsv.2007.01.003.

12. Nanda N., Bandyopadhyay J.N., Nonlinear free vibration analysis of laminated composite cylindrical shells with cutouts, *Journal of Reinforced Plastics and Composites*, **26**(14): 1413–1427, 2007, doi: 10.1177/0731684407079776.

13. Sahoo S., Free vibration of laminated composite hypar shell roofs with cutouts, *Advances in Acoustics and Vibration*, **2011**: Article ID 403684, 2011, doi: 10.1155/2011/403684.

14. Chaubey A.K., Kumar A., Chakrabarti A., Vibration of laminated composite shells with cutouts and concentrated mass, *AIAA Journal*, **56**(4): 1662–1678, 2018, doi: 10.2514/1.J056320.

15. Kulikov G.M., Plotnikova S.V., Advanced formulation for laminated composite shells: 3D stress analysis and rigid-body motions, *Composite Structures*, **95**: 236–246, 2013, doi: 10.1016/j.compstruct.2012.07.020.

16. Talebitooti R., Zarastvand M.R., Gheibi M.R., Acoustic transmission through laminated composite cylindrical shell employing third order shear deformation theory in the presence of subsonic flow, *Composite Structures*, **157**: 95–110, 2016, doi: 10.1016/j.compstruct.2016.08.008.

17. Tornabene F., Fantuzzi N., Bacciocchi M., The local GDQ method for the natural frequencies of doubly-curved shells with variable thickness: a general formulation, *Composites Part B: Engineering*, **92**: 265–289, 2016, doi: 10.1016/j.compositesb.2016.02.010.

18. Tornabene F., Fantuzzi N., Bacciocchi M., The GDQ method for the free vibration analysis of arbitrarily shaped laminated composite shells using a NURBS-based isogeometric approach, *Composite Structures*, **154**: 190–218, 2016, doi: 10.1016/j.compstruct.2016.07.041.

19. Wang Q., Shi D., Liang Q., Pang F., Free vibrations of composite laminated doubly-curved shells and panels of revolution with general elastic restraints, *Applied Mathematical Modelling*, **46**: 227–262, 2017, doi: 10.1016/j.apm.2017.01.070.

20. Tornabene F., Fantuzzi N., Bacciocchi M., Reddy J.N., An equivalent layer-wise approach for the free vibration analysis of thick and thin laminated and sandwich shells, *Applied Sciences*, **7**(1): 17, 2016, doi: 10.3390/app7010017.

21. Chaudhuri P.B., Mitra A., Sahoo S., Mode frequency analysis of antisymmetric angle-ply laminated composite stiffened hypar shell with cutout, *Mechanics and Mechanical Engineering*, **23**(1): 162–171, 2019, doi: 10.2478/mme-2019-0022.

22. Reddy J.N., *Energy and Variational Methods in Applied Mechanics*: *with an Introduction to the Finite Element Method*, John Wiley, New York, 1986.

23. Chandrashekhara K., Free vibrations of anisotropic laminated doubly curved shells, *Computers & Structures*, **33**(2): 435–440, 1989, doi: 10.1016/0045-7949(89)90015-1.

24. Leissa A.W., Qatu M.S., Equations of elastic deformation of laminated composite shallow shells, *Journal of Applied Mechanics*, **58**(1): 181–188, 1991, doi: 10.1115/1.2897146.

25. Vasiliev V.V., Jones R.M., Man L.I., *Mechanics of Composite Structures*, Taylor & Francis, USA, 1993.

26. Qatu M.S., *Vibration of Laminated Shells and Plates*, Elsevier, UK, 2004.

27. Sahoo S., Laminated composite stiffened cylindrical shell panels with cutouts under free vibration, *International Journal of Manufacturing, Materials, and Mechanical Engineering (IJMMME)*, **5**(3): 37–63, 2015, doi: 10.4018/IJMMME.2015070103.

28. Mukherjee A., Mukhopadhyay M., Finite element free vibration of eccentrically stiffened plates, *Computers & Structures*, **30**(6): 1303–1317, 1998, doi: 10.1016/0045-7949(88)90195-2.

29. Nayak A.N., Bandyopadhyay J.N., On the free vibration of stiffened shallow shells, *Journal of Sound and Vibration*, **255**(2): 357–382, 2002, doi: 10.1006/jsvi.2001.4159.

30. Chakravorty D., Sinha P.K., Bandyopadhyay J.N., Applications of FEM on free and forced vibration of laminated shells, *Journal of Engineering Mechanics*, **124**(1): 1–8, 1998, doi: 10.1061/(ASCE)0733-9399(1998)124:1(1).

Received October 15, 2022; accepted version January 2, 2023.